Pergamon

Acta Materialia 50 (2002) 2989–3002

Acta MATERIALIA

www.actamat-journals.com

Polarization switching in $PbTiO_3$: an ab initio finite element simulation

E.B. Tadmor [a,*], U.V. Waghmare [b 1], G.S. Smith [b], E. Kaxiras [b]

[a] *Faculty of Mechanical Engineering, Technion — Israel Institute of Technology, 32000 Haifa, Israel*
[b] *Department of Physics, Harvard University, Cambridge, MA 02138, USA*

Received 26 September 2001; received in revised form 14 February 2002; accepted 14 March 2002

Abstract

A continuum constitutive model for $PbTiO_3$ has been obtained from an effective Hamiltonian which was constructed from ab initio calculations. This model contains the nonlinearities necessary for switching from the ground-state tetragonal phase to the metastable rhombohedral and orthorhombic phases. The constitutive model was incorporated into a finite element formulation in order to study the large length-scale electro-mechanical response of this piezoelectric material. We use this approach to study the hysteresis of single-crystal $PbTiO_3$ as a function of applied electric field and temperature and we analyze the microscopic mechanisms responsible for polarization switching. The model successfully reproduces the qualitative features of a high-strain actuator recently proposed and tested experimentally. © 2002 Acta Materialia Inc. Published by Elsevier Science Ltd. All rights reserved.

Keywords: Computer simulation; Ab initio calculation; Functional ceramics; Ferroelectricity; Polarization switching

1. Introduction

Ferroelectric materials are becoming increasingly important both in the microelectronics industry and the emerging field of microelectromechanical systems (MEMS). A ferroelectric material exhibits a spontaneous polarization in a direction that can be switched by the application of an external electric field or stress [1]. This phenomenon is a manifestation of the strong coupling between mechanical strain and electric field, and nonlinearity in the constitutive response of these materials. The linear coupling corresponds to the *piezoelectric* effect and the quadratic coupling corresponds to the *electrostrictive* effect. In microelectronics, the switchability of ferroelectrics is exploited in the design of nonvolatile ferroelectric random-access memories (NVFRAM's) [2], which can retain stored data without the need for external power. In MEMS applications, the electrostrictive/piezoelectric nature of ferroelectrics is utilized in the design of highly accurate microscopic sensors and actuators [3,4].

In both of these areas, as Hwang and McMeeking [5] pointed out, there is growing need for the

* Corresponding author: Tel.: +972 4 829 3466; fax: +972 4 829 4573.
E-mail address: tadmor@tx.technion.ac.il (E.B. Tadmor).
[1] Current address: Theoretical Sciences Unit, Jawaharlal Nehru Centre for Advanced Scientific Research, Bangalore 560064, India.

1359-6454/02/$22.00 © 2002 Acta Materialia Inc. Published by Elsevier Science Ltd. All rights reserved.
PII: S1359-6454(02)00127-1

development of accurate models for the nonlinear response of ferroelectrics subjected to arbitrary applied electric field and stress. Although the nominal operating stresses of ferroelectric devices may be low, in practice large stresses and strains, outside of the linear regime, are often encountered as a result of domain reorientation during switching [5] and in the vicinity of device edges and defects [6]. Due to the lack of predictive nonlinear models, current actuator design is limited to the linear regime, which constitutes only a small fraction of the entire range available to ferroelectric materials [5].

In the past, simulations of piezoelectric materials have been primarily limited to small strains and electric fields where a linear model of material response is adequate [7,8]. Most recent work on the development of nonlinear constitutive models for ferroelectrics has focused on electrostrictive materials such as lead magnesium niobate $Pb(Mg_{1/3}Nb_{2/3})O_3$ (PMN) [9,10,11,12]. The models are phenomenological in nature; they are formulated to capture the quadratic dependence of strain on electric displacement and the saturation of polarization at large electric field, but they neglect hysteresis.

For piezoelectric materials several different approaches have been proposed. A phenomenological power-law model relating deviatoric stress to deviatoric strain was proposed by Cao and Evans [6]. The use of a deviatoric model was based on the observation that the volume change behaved linearly with applied load, indicating that the nonlinear behavior was tied to the deviatoric components of the stress and strain. The power-law form was fitted to the experimental results for several different materials. This model also neglects hysteretic effects. A micromechanical model for piezoelectric ferroelectrics was proposed by Hwang and McMeeking [5] and Chen and Lynch [13] for lead lanthanum zirconate titanate $Pb_{1-x}La_x(Zr_yTi_z)_{1-x/4}O_3$ (PLZT). In this approach, a polycrystalline sample is represented as a collection of uniformly polarized crystallites with random crystallographic orientation. For perovskite ferroelectrics with tetragonal symmetry, like PLZT and $PbTiO_3$, there are six possible states of polarization. One of these is selected randomly for each of the crystallites. A linear model is used to characterize the response of the crystallite about its polarized state and a phenomenological criterion is used to trigger switching to other possible states. A similar micromechanical approach based on the internal variable theory has been advanced by Chen et al. [14].

At a more fundamental level, atomistic ab initio calculations based on density-functional-theory (DFT) have been very successful in obtaining a wide range of properties of ferroelectric materials [15] including domain wall energies, elastic constants and dielectric and piezoelectric coefficients. The advantage of the DFT methods is that they yield an unbiased model for material-specific properties through access to accurate microscopic energetics with no empirical input.

In this paper we attempt to draw upon the strengths of both the continuum approaches which allow for the modeling of macroscopic systems and the atomistic models which retain microscopic information. We focus on lead titanate $PbTiO_3$, an end-member of the technologically important family of ferroelectric materials $Pb(Zr_xTi_{1-x})O_3$ (PZT). To this end, we incorporate the ab initio model developed by Waghmare and Rabe [16] to simulate the ferroelectric phase transition in $PbTiO_3$ within the complex-crystal finite element formulation that we have recently developed [17]. We use this approach to simulate the nonlinear hysteretic response of $PbTiO_3$ at the macroscopic scale and to study the microscopic mechanisms responsible for polarization switching. We also study the behavior of a high-strain actuator under large external electric field and mechanical pressure.

2. An effective Hamiltonian for $PbTiO_3$

The piezoelectric material $PbTiO_3$ has a noncentrosymmetric tetragonal crystal structure, with a spontaneous polarization along the *c*-axis ([001] direction). The simplest hysteresis experiment involves reversing the direction of spontaneous polarization with an application of electric field. Similarly, application of stress can switch the polarization direction to [100] or [010]. The resulting six polarization states have the same point group

symmetry with different crystallographic orientations. They are most easily described as strained and internally distorted forms of the cubic perovskite structure (see Fig. 1), i.e. the structure of paraelectric $PbTiO_3$ occurring at elevated temperatures.

In order to model the behavior of $PbTiO_3$ within a finite element method [17] it is necessary to have a quantitatively accurate description of the energetics as a function of strain and electric field. An effective Hamiltonian that describes six equivalent states of $PbTiO_3$ and switching among them is bound to be highly nonlinear. Noting that the six states occur in three pairs and that two states in each pair have polarization with opposite directions, it is clear that the energetics are also a function of polarization and that the nonlinearity is primarily in the dependence of the energy on polarization.

In modern theory, polarization is defined with respect to a reference nonpolar state and is a function of parameters that relate a crystal to the reference state [18,19]. In the present context, the paraelectric state of $PbTiO_3$ is a natural choice for the reference nonpolar structure, with the internal atomic displacements and the macroscopic strain being the appropriate parameters. Thus, the effective Hamiltonian can be expressed naturally as a Taylor expansion in strain and internal atomic displacements with respect to the cubic paraelectric structure. To keep the form of the effective Hamiltonian simple, but sufficient to span the neighborhood of these states and the energy barriers separating them, we express it as a Taylor expansion in the Lagrangian finite strain $\mathbf{e}$ [20], the electric field $\mathbf{E}$, and $\boldsymbol{\xi}$ which is a linear combination of atomic displacements that relate the piezoelectric states to the lowest-energy distortions of the cubic structure [16]. The atomic positions within the cubic unit cell for $\boldsymbol{\xi}= (0,0,\xi_z)$ are given in Table 1. Atomic positions for $\boldsymbol{\xi}$ in other directions are obtained by appropriate symmetry transformations (for details see Ref. [16]). With the parameters defined above, the tetragonal ground state oriented along the z-axis is given by: $\boldsymbol{\xi}=(0,0,0.086)$, $e_{xx}=e_{yy}=-0.0168$ and $e_{zz}=0.0706$.

An explicit form of the effective Hamiltonian is obtained by requiring it to be invariant under cubic symmetry and making use of the symmetry proper-

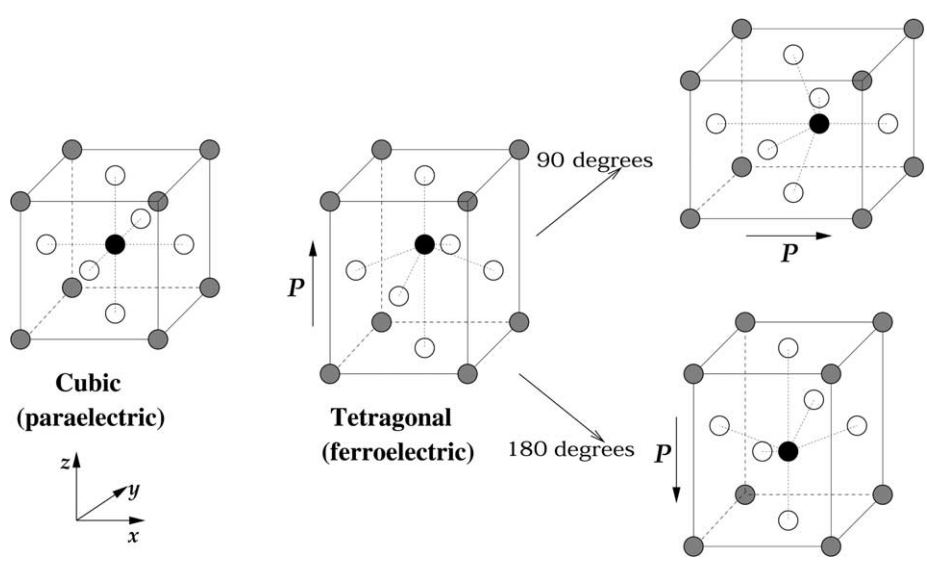

Fig. 1. Perovskite crystal structure of $PbTiO_3$: Atoms at the corner of the unit cell are Pb (gray), ones at the center of faces are O (white) and the one at the center of the cell is Ti (black). Above T=760 K, the structure has cubic symmetry corresponding to paraelectric phase and at low temperature, it becomes non-centrosymmetric tetragonal corresponding to the ferroelectric (piezoelectric) phase. The transition between the two phases is of first-order and is characterized by a nonzero order parameter, polarization **P**, in the ferroelectric phase. Application of external stress or electric field can cause 90 or 180 degree switching of the tetragonal phase to symmetry-related states.

Table 1
Normalized coordinates of the atoms within the cubic unit cell for the case $\boldsymbol{\xi}=(0,0,\xi_z)$

Atom	Coordinates
Pb	(0, 0, $0.5560\xi_z$)
Ti	(0.5, 0.5, $0.5-0.5375\xi_z$)
O[011]	(0, 0.5, $0.5-0.3414\xi_z$)
O[101]	(0.5, 0, $0.5-0.3414\xi_z$)
O[110]	(0.5, 0.5, $-0.4109\xi_z$)

ties of $\mathbf{e}$ and $\boldsymbol{\xi}$. The energy density $\mathbf{E}_{\text{tot}}$ is thus given by:

$$\begin{aligned}\varepsilon_{\text{tot}}(\mathbf{e},\boldsymbol{\xi},\mathbf{E}) &= \frac{1}{2}C_{11}\sum_{\text{i}} e_{\text{ii}}^2 + \frac{1}{2}C_{12}\sum_{\text{i}\neq\text{j}} e_{\text{ii}}e_{\text{jj}} \\ &+ \frac{1}{4}C_{44}\sum_{\text{i}\neq\text{j}} e_{\text{ij}}^2 + f\sum_{\text{i}} e_{\text{ii}} + g_0|\boldsymbol{\xi}|^2\sum_{\text{i}} e_{\text{ii}} \\ &+ g_1\sum_{\text{i}} e_{\text{ii}}\xi_{\text{i}}^2 + \frac{1}{2}g_2\sum_{\text{i}\neq\text{j}} e_{\text{ij}}\xi_{\text{i}}\xi_{\text{j}} + \tilde{h}_0|\boldsymbol{\xi}|^2 \\ &+ h_1|\boldsymbol{\xi}|^4 + h_2(\boldsymbol{\xi}_{\text{x}}^4 + \boldsymbol{\xi}_{\text{y}}^4 + \boldsymbol{\xi}_{\text{z}}^4) + h_3|\boldsymbol{\xi}|^6 \\ &+ h_4|\boldsymbol{\xi}|^8 - \frac{Z}{a_0^2}\sum_{\text{i}}\boldsymbol{\xi}_{\text{i}}E_{\text{i}} - \frac{1}{8\pi}\varepsilon^{\infty}\sum_{\text{i}}E_{\text{i}}^2,\end{aligned} \tag{1}$$

where C_{ij} are elastic constants, f is the stress needed to compensate for the standard Local Density Approximation (LDA) error in the lattice constant, g_{i} are the couplings between strain and atomic displacements, $\tilde{h}_0$ is the harmonic force constant for $\boldsymbol{\xi}$, h_1 through h_4 are anharmonic coefficients, Z is the mode effective charge, a_0 is the lattice parameter and ε^{∞} is the dielectric constant. All indices appearing in Eq. (1) run from 1 to 3. The expansion in Eq. (1) is the projection of the model developed in Ref. [16] onto the subspace of uniform atomic displacements mapped by $\boldsymbol{\xi}$ with appropriate terms added to allow for interaction with the applied electric field. The nonlinearity in energy is evident in the anharmonic terms in the variable $\boldsymbol{\xi}$. The polarization is given by:

$$P_{\text{i}} = \frac{Z}{\Omega}\xi_{\text{i}} + \frac{1}{4\pi}(\varepsilon^{\infty}-1)E_{\text{i}}, \tag{2}$$

where Ω is the volume of the cubic unit cell.

Due to the finite temperature ferroelectric phase transition in $PbTiO_3$ (also linked to strong anharmonicity), its dielectric and piezoelectric response is strongly temperature dependent. The present approach can be readily generalized to finite temperature (T) through a free energy expansion. Due to symmetry, the form of the expansion remains the same, with the parameters being temperature dependent. In the present work, we use the phenomenological arguments of Landau's mean field theory [21] to absorb the temperature dependence in the $\tilde{h}_0$ parameter alone,

$$\tilde{h}_0(T) = h_0\left(1-\frac{T}{T_0}\right), \tag{3}$$

with $\tilde{h}_0(0)=h_0$, used in the ground state energy expansion. The parameter T_0 is obtained by fitting the temperature dependence of the polarization obtained from Monte Carlo simulations [16]; its value is T_0=1028 K.

The remaining parameters appearing in this model have all been obtained from total energy and linear-response calculations based on DFT. The computed values are given in Table 2 for the following unit convention: e_{ij} and ξ_{i} are dimensionless and E_{i} is measured in eV/Å. Additional parameters are a_0=3.969 Å, Z=10.0151 e and ε^{∞}=8.24. This approach involves no empirical input and allows systematic testing through overdetermination of these parameters.

3. Finite element method implementation

The effective Hamiltonian presented in the previous section characterizes the response of an infinite crystal subjected to uniform loading. To study the response of more complex nonhomogeneous systems, we have implemented the model within the 3D finite element method (FEM) formulation for complex crystals, which has recently been developed by the authors [17]. This is a standard Lagrangian finite-strain FEM formulation with the exception that the constitutive relation characterizing the material response is obtained from atomistic models. In the present case, the effective

Table 2
Parameters appearing in the effective Hamiltonian. Units are in eV/Å^3 for all parameters

C_{11}	1.886	g_0	−0.1094	h_0	−0.4808	h_3	-2.652×10^3
C_{12}	0.8238	g_1	−0.8026	h_1	42.05	h_4	1.540×10^5
C_{44}	2.195	g_2	−0.2590	h_2	68.42	f	7.166×10^{-2}

Hamiltonian of Eq. (1) which was obtained from first-principles calculations serves as that model. Since the formulation is designed with complex crystals in mind, each element has degrees of freedom associated with it corresponding to the positions of the internal unit-cell atoms. The total energy is minimized with respect to these degrees of freedom as well as the nodal degrees of freedom. For $PbTiO_3$ there are four atoms per unit cell free to relax (the fifth atom serves as the origin of the coordinate system) which produces 12 additional degrees of freedom per finite element. However, using the reduced description in terms of the variable $\boldsymbol{\xi}$, only three additional degrees of freedom need to be explicitly treated.

The use of the above model in a FEM formulation is facilitated by an appropriate variational principle. In addition to mechanical boundary conditions [17], electric boundary conditions need to be imposed in a simulation of a piezoelectric material. While the general electric boundary conditions can be specified with a scalar potential and charges at the boundary, in this work we restrict our attention to the special case of closed-circuit boundary conditions. The closed-circuit boundary conditions are imposed by requiring that the macroscopic electric field in the sample be constant. In an experiment, this corresponds to having electrodes at the boundary which supply free carriers at the surface to compensate for the depolarizing fields. Free charge carriers are assumed to compensate for variations in the polarization field in the bulk of the piezoelectric. The variational principle for this case is given by,

$$\left.\frac{\partial \Pi}{\partial \xi_i}\right|_E = 0 \quad \text{and} \quad \left.\frac{\partial \Pi}{\partial e_{ij}}\right|_E = 0, \tag{4}$$

where Π is the total potential energy of the system. For closed-circuit conditions,

$$\Pi = \int_V \varepsilon_{tot} dV - W, \tag{5}$$

where V is the system volume and W is the work of the external tractions.

In a finite element simulation, the above energy function is minimized with respect to $\boldsymbol{\xi}$ for each element and the total energy of the full sample is subsequently minimized with respect to strain (for details see Ref. [17]). In the current formulation, all minimizations were carried out using a conjugate gradient (CG) algorithm. Minimization with respect to $\boldsymbol{\xi}$ used a standard CG-solver and minimization with respect to **e** used a preconditioned CG-solver to accelerate convergence. In this case, the simplest form of preconditioning was used, referred to as diagonal scaling preconditioning [22], in which the force gradient is normalized by the diagonal elements of the second-derivative matrix (the Hessian) of the total energy. Since the effective Hamiltonian is highly nonlinear, it has a large number of local minima in both **e** and $\boldsymbol{\xi}$-space. In a simulation, energy minimization is performed to the local minimum nearest to the previous configuration.

4. Polarization switching under uniform loading

We first illustrate the application of our approach to polarization switching (hysteresis) in $PbTiO_3$. This phenomenon is the basis for use of ferroelectric materials in NVFRAM's. Due to the tetragonal symmetry of the $PbTiO_3$ crystal, there are six possible orientation states of polarization which have the same energy and are related to each other by symmetry operations such as rotation and reflection. There are two mechanisms for switching

between these states (see Fig. 1): rotations through 90° and inversion (equivalent to a 180° rotation). Switching can be induced by application of an external electric field or stress. The energetics of these mechanisms, such as the energy barriers along paths connecting any two states, fall out of the model discussed above.

To understand the switching mechanisms, we first simulate a single-crystal $PbTiO_3$ sample constituting a single polarized domain. The crystal is unconstrained mechanically (beyond prevention of rigid-body motion) and is subjected to closed-circuit electric boundary conditions (**E**=constant). In Fig. 2, we show the change in polarization in response to a saw-tooth electric field with an amplitude of 200 MV/m which is applied parallel to the *c*-axis (the direction of spontaneous polarization). Clearly, the polarization response is strongly nonlinear and history dependent. A strong enough electric field applied against the direction of polarization switches its sign. The magnitude of the switching field is strongly temperature dependent (156 MV/m at 0 K and 91 MV/m at 300 K). Its magnitude reduces as the temperature approaches the ferroelectric phase transition from below and is zero on the other side of this transition, where the polarization vanishes due to the symmetry of the high-temperature phase. The polarization at zero applied electric field is the spontaneous polarization which our model predicts to be 0.87 C/m^2 at zero temperature (0.73 C/m^2 at room temperature), in good agreement with the experimental value of 0.5–1.0 C/m^2 [23].

To our knowledge there are no experimental results available for switching in single crystal $PbTiO_3$. Switching fields known from experiments in PZT systems are an order of magnitude smaller than the ones we find [24]. In part, this is due to the fact that in the simulation switching is homogeneous, while in the physical sample switching occurs with a nucleation event. Similar results were obtained by Landauer et al. [25] who estimated the coercive switching field for homogeneous switching in $BaTiO_3$ based on Devonshire theory. The predicted field was found to be roughly 20 MV/m which, as in our case, is two orders of magnitude larger than experimental values. An additional reason for the discrepancy with experimental results for PZT is that the PZT system is very close to the phase transition with respect to composition (i.e. near the morphotropical phase boundary). Such proximity should substantially reduce the switching field and stress just as we find in the case of temperature dependence. The 180° switching described above is accompanied by homogeneous straining of the unit cell of the $PbTiO_3$ crystal. In Fig. 2 we also show the strain

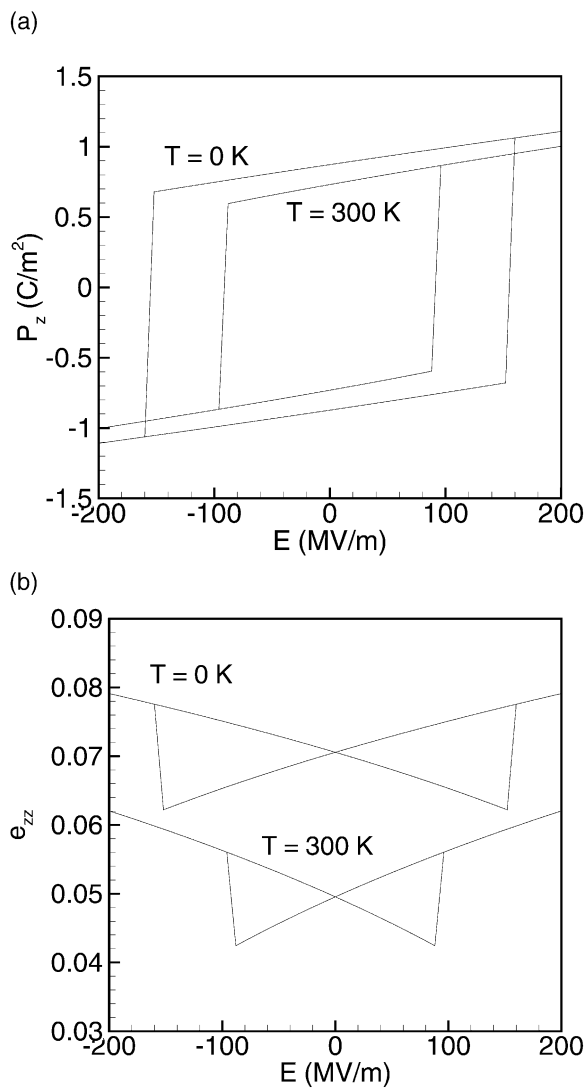

Fig. 2. Polarization and strain response for 180° switching in single-crystal $PbTiO_3$ due to a saw-tooth electric field **E** applied anti-parallel to the direction of polarization.

component e_{zz} as a function of the applied electric field. The butterfly shape diagrams are qualitatively similar to the ones seen in experiment in other related materials such as PLZT [5].

To probe the microscopic mechanism responsible for switching, we use the elastic band method [26] to explore the transition path the system may follow and the associated energy barrier(s)[2]. In Fig. 3, we display the degrees of freedom $\boldsymbol{\xi}$ and **e** as functions of the transition coordinate. It is clear that the transition path starts with a tetragonal phase, passes through an orthorhombic phase at the quarter point and reaches another tetragonal phase, oriented perpendicular to the initial phase, at the halfway point. In the second half, it passes through another orthorhombic phase to reach the tetragonal phase oriented 180° with respect to the initial phase. Thus, the 180° switching of polarization (polarization reversal) consists of two 90° rotations. The transition path in Fig. 3 was computed for the case of no applied electric field at 0 K. At the switching field (E_z=156 MV/m), we find an essentially identical transition path with the exception that there is a slight offset due to the presence of the electric field.

In Fig. 4, we show the energy along the transition path at zero electric field (at the switching field, the barrier for switching vanishes, of course). The transition path discussed above has energy barriers (ΔE=7.8 meV per unit cell or 0.125 meV/Å^3) at the quarter and three-quarters points of the path, corresponding to the orthorhombic phases. We also probed the energetics of the path when tetragonal symmetry is enforced. This path passes through a high energy barrier (ΔE=105 meV per unit cell) at the halfway point corresponding to the cubic phase. Thus, our results show that the barrier for switching via 90° rotation is 13.5 times smaller than that for the straight 180° switching.

These results may be compared to the switching barriers used in the work of Hwang and McMeeking [5] for PLZT. In that case, a phenomenological model was used and the switching barriers were

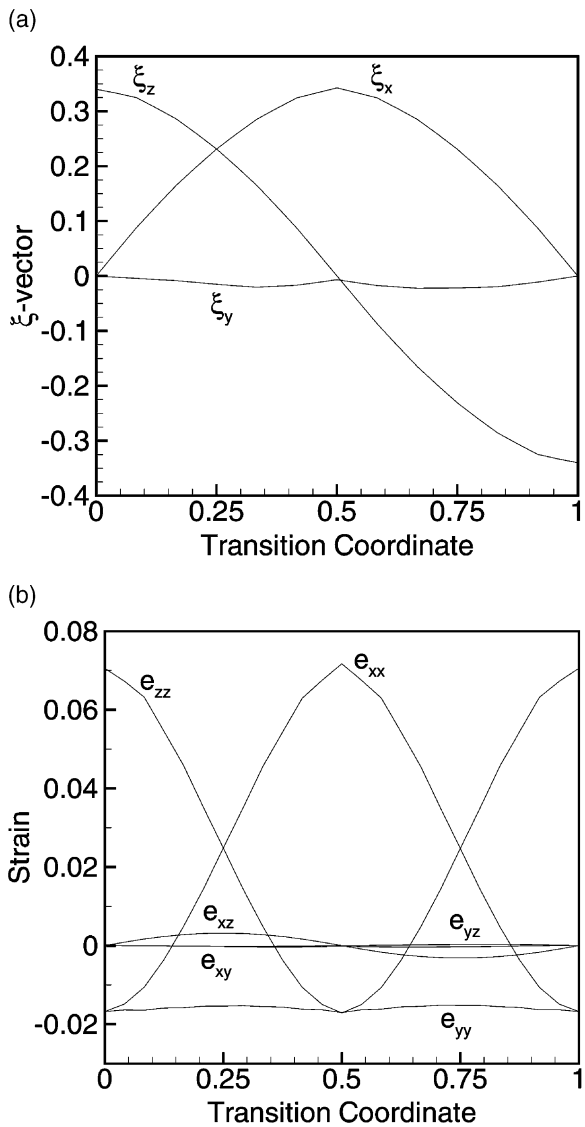

Fig. 3. $\boldsymbol{\xi}$-value (proportional to polarization) and strain variation across a 180° switch in single-crystal $PbTiO_3$ obtained by an elastic band calculation.

obtained by fitting the model predictions to experiment. The authors find that 90° switching is the dominant mechanism with a barrier of about 5×10^{-4} meV/Å^3. The barrier for 180° switching is set arbitrarily high in order to discourage that mechanism. Our first-principles results clearly reinforce the conclusion regarding the relative magnitudes of 90° and 180° switching barriers.

[2] It is important to note that the transition path identified by the elastic band method does not account for the kinetics of the switching process and thus may not be the one actually taken by the physical system.

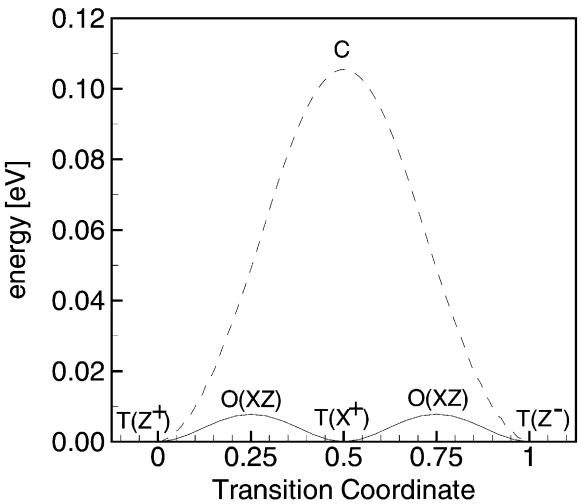

Fig. 4. Energy per unit cell across a 180° switch in single-crystal $PbTiO_3$ obtained by an elastic band calculation. The solid line is the relaxed elastic band transition path. The dashed line is the transition path when tetragonal symmetry is enforced during the switch. The letters correspond to different phases along the transition path (T=Tetragonal, O=Orthorhombic, C=Cubic).

However, quantitatively, the barrier heights are very different. As in the results of the coercive field discussed earlier, this discrepancy is partly due to the difference between materials and partly due to the fact that the experimental system most likely switches nonuniformly through domain nucleation and domain wall motion. The barrier height obtained in Ref. [5] is thus an effective barrier that captures the complex experimental behavior.

When tetragonal symmetry is enforced during the switch, the resulting switching fields are found to be much higher (460 MV/m at 0 K and 280 MV/m at 300 K). This is surprising since application of a uniform electric field in the direction of polarization would not be expected to break the crystal symmetry. In practice, maintaining tetragonal symmetry across the switch results in a metastable path across a saddle ridge in energy space. This was established by studying the eigenvalues of the Hessian across the transition path. It was found that the Hessian loses positive definiteness, indicating that the symmetric transition path is metastable.

The process of 90° switching which was found to be important in polarization reversal can also be induced by applying an electric field perpendicular to the polarization direction or by applying an external stress parallel to the direction of polarization. A small electric field applied perpendicular to the polarization direction results in an initial linear response of polarization parallel to the field. As the field is increased, the response becomes nonlinear and there is a discontinuous jump resulting in zero polarization along the *c*-axis and a nonzero polarization equal to the spontaneous polarization parallel to the field. The direction of polarization has been rotated by 90°. The switching field is found to be 52 MV/m, a factor of three smaller than that for 180° switching. It is very interesting that the same energy landscape (determined by the effective Hamiltonian) underlying the two switching processes gives rather different values for the switching fields. The reason for this is that the perpendicular applied field breaks tetragonal symmetry and thus favors the intermediate orthorhombic phases, whereas the parallel field preserves this symmetry. 90° switching due to applied stress is qualitatively different. Unlike the electric field, the applied stress does not break the tetragonal symmetry of the crystal. Hence, the polarization response in the perpendicular direction is zero until there is a switch to a 90° rotated state at large applied stress. The switching stress is about 0.9 GPa. Experimental switching stresses for related materials are significantly smaller (about an order of magnitude less). The reasons for the discrepancy are the same as those mentioned for the coercive field and the switching barrier.

5. Simulations of single-crystal actuators

A second important application of ferroelectric materials is actuation. In this section, we simulate the behavior of a large-strain ferroelectric actuator proposed by Shu and Bhattacharya [27]. The basic idea of their proposal is illustrated in Fig. 5. A stress is applied along the the *z*-axis to a single crystal ferroelectric with a (100) orientation, switching the polarization into the *xy* plane. The actuator is then controlled by an electric field applied along the *z*-axis. For a sufficiently large

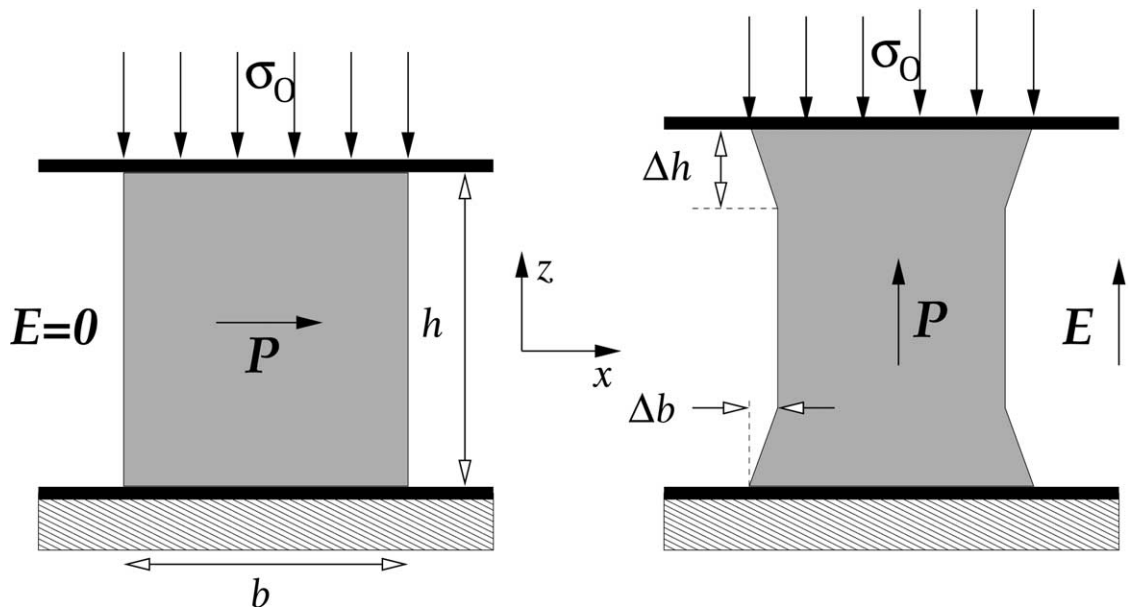

Fig. 5. Schematic diagram of the proposed high strain actuator of Shu and Bhattacharya [27]. A normal stress σ_0 is applied to a ferroelectric sample, and an applied electric field is used to switch between a configuration with polarization in the *xy* plane, and polarization in the *z* direction. The figure also includes dimensions used in a qualitative model developed later to explain the length scale of the effect due to surface pinning observed in the simulations.

applied field, the polarization of the sample aligns with the electric field. This switch of polarization is accompanied by a large strain as the long axis of the tetragonal unit cell moves out of the *xy* plane to align itself with the *z*-axis. When the electric field is reduced, polarization switches back to the *xy* plane, and the original configuration is recovered.

Using our simulation method with closed-circuit boundary conditions (**E** does not vary spatially) we explore how the system behaves for different applied stresses when the electric field is cycled. We also consider how friction between the plates through which the external stress is applied, and the surface of the ferroelectric sample, affects the behavior. The simulations are carried out in three dimensions. We compare our results with the experimental work of Burcsu et al. [4], which investigates the actuator design proposed in Ref. [27]. Though they used a different material ($BaTiO_3$), we will still be able to compare the qualitative features of our simulation with their experiments.

We consider the behavior of a single-crystal slab of $PbTiO_3$ in the setup illustrated in Fig. 5, under a cycled electric field. We assume first that the surfaces of the sample are unconstrained. Our simulated piezoelectric sample is a cube with six finite elements. Since there is no friction between the plates and the sample, the strain field is uniform and there is no reason to use a larger mesh. We checked explicitly that the results do not depend significantly on the aspect ratio of the sample or on the number of finite elements. Fig. 6 shows the polarization and strain vs. electric field for different applied stress levels. All the simulations begin with the external electric field set to zero and the external stress applied to the paraelectric phase which forces the sample into the tetragonal phase with polarization in the *xy* plane. In a given simulation, the polarization of all the finite elements is either randomly distributed among the $+x$ and $-x$ directions, or among the $+y$ and $-y$ directions: there is no mixture of *x* and *y* directions due to the associated cost in elastic energy. The electric field is then incrementally increased. At a sufficiently large electric field, the polarization of the sample aligns with the $+z$ direction. After reaching its maximum

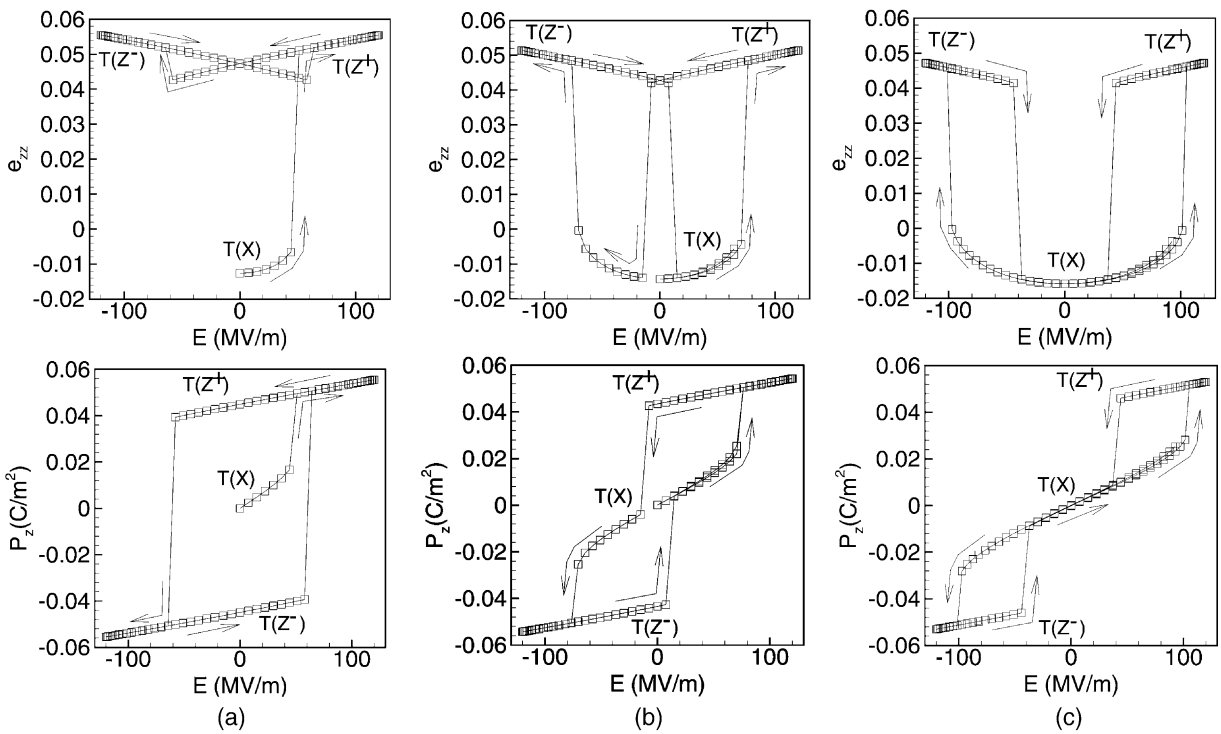

Fig. 6. Strain and polarization vs. electric field curves for three different applied stress values: (a) σ_0=100 MPa, (b) σ_0=300 MPa and (c) σ_0=500 MPa. There is no friction between the plates and the $PbTiO_3$ sample. The notation of the phases is the same as in Fig. 3.

magnitude, the electric field begins decreasing, and the subsequent behavior depends on the magnitude of the applied stress. Two different behaviors are apparent. In Fig. 6(a), which corresponds to the lowest applied stress (σ_0=100 MPa), the distinctive parallelogram curve for the polarization P_z and the butterfly curve for the strain e_{zz}, already seen in Fig. 2, are obtained. Here the polarization switches between the $+z$ and $-z$ directions. For the systems subject to larger stresses in Fig. 6(b) and (c), the large strain actuation is achieved. In these cases, the stress is sufficiently large so that a stable configuration with polarization in the *xy* plane is available for the system to fall into when polarization aligned with the *z*-axis becomes unstable.

The simulated strain vs. electric field curves can be compared with the experimental results of Burcsu et al. [4] for $BaTiO_3$. The general shape of Fig. 6(b) is similar to that of the experimental curve. There is some decay in the experimental curve due to degradation of the sample during electric field cycling which is absent in the simulation where such effects are not included. In the experiment, for an applied stress of 3.6 MPa, the switching field is about 1 MV/m and the actuation strain is 0.008. The simulation uses the effective Hamiltonian for $PbTiO_3$, while the experiment concerns the behavior of $BaTiO_3$; this explains the difference in the scale of the strain axis. The difference in scale of the electric field and stress values is primarily due to the fact that in the simulation, switching is homogeneous, while in experiment it occurs by nucleation and expansion of domain walls between regions of different polarization.

In the simulations discussed thus far, there has been no friction between the sample surface and the plates. Friction is part of the experimental system and perhaps plays an important role. Burcsu et al. suggested that friction between the plates and the sample may have contributed to the inability

of their actuators to achieve the maximum possible strain [4]. We explore the effect of friction by applying perfect stick boundary conditions to the surfaces. At the beginning of a simulation, after applying the external stress to force the polarization into the *xy* plane, the surface where the stress is applied is pinned so that it can no longer move in the *x* or *y* direction as the electric field is cycled. Fig. 7 shows the simulated strain vs. electric field curve for this case at a stress of 300 MPa, compared with the curve for the unconstrained case which also appears in Fig. 6(b). With the surface pinned, switching cannot occur near the surface, so the change in strain when the sample switches between polarization states is smaller than when the surface is free. The switching field from the configuration with polarization in the *xy* plane to polarization in the *z* direction is nearly the same in both cases. However, the elastic penalty due to the alignment of the middle of the pinned sample with the electric field, causes it to switch back to the configuration with polarization in the *xy* plane earlier than the unconstrained sample as the electric field is decreasing.

An important detail is that in the simulation used to produce Fig. 7 the height-to-base aspect ratio of the sample is large: the height of the sample in the *z* direction is twice the base dimension in the *xy* plane. If the height is increased further relative to the base dimension, surface effects become increasingly unimportant, and the results approach those of the case when the surface is free (see Fig. 6). If the height is decreased relative to the base dimension, then switching becomes increasingly difficult. When the height is equal to the base dimension, there is no switching from the initial configuration over the range of electric fields considered in Fig. 6.

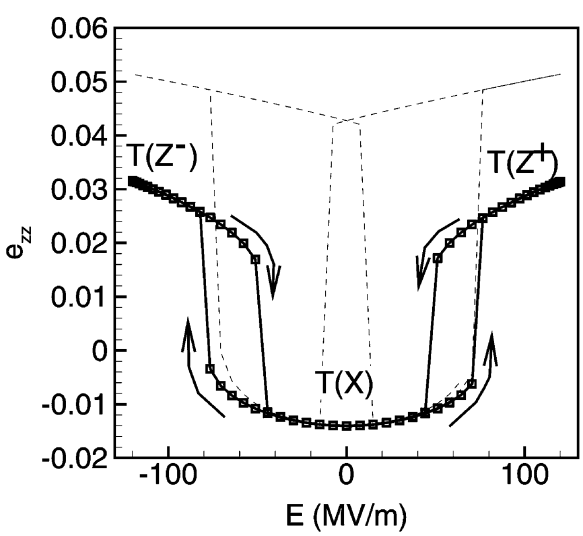

Fig. 7. Strain vs. electric field curve when the surfaces of the sample are not permitted to move in the *xy* plane (solid line with symbols) compared with the unconstrained case (dashed line). The external stress is set to 300 MPa.

In order to explore this issue further and to obtain a better understanding of the polarization patterns that form when the surfaces are pinned, we show in Fig. 8 the polarization of the individual finite elements in the absence of an electric field and with the electric field at its maximum value, 120 MV/m. When the electric field is zero, Fig. 8(a), the polarization of the individual finite elements is in the $+x$ and $-x$ directions. At the maximum value of the field, Fig. 8(b), the polarization in the regions adjacent to the plates is close to being in the *xy* plane; moving towards the interior of the sample the polarization rotates smoothly to align with the external electric field. The asymmetry in the *z* direction is a result of the different boundary conditions applied on the top and bottom surfaces; the bottom surface was held completely fixed, while the top was fixed in the *x* and *y* directions, but allowed to move in the *z* direction. In the middle, the sample bows in since the central switched region has the narrower dimension of the tetragonal unit cell in the *xy* plane, while the region near the plates has the longer dimension of the tetragonal unit cell in the *xy* plane. The change in length in the *z* direction, which is the basis of the actuation, is also visible. The length scale of the effect due to the surface pinning, which we denote by Δh, is on the order of the base dimension.

To understand what determines the length scale Δh, we construct a simple expression for the energy at a fixed electric field for a sample with a central switched region as in Fig. 8(b). The length scale Δh is determined by minimizing this energy. Fig. 5 shows a schematic of the sample, and the quantities that will be used to analyze the ener-

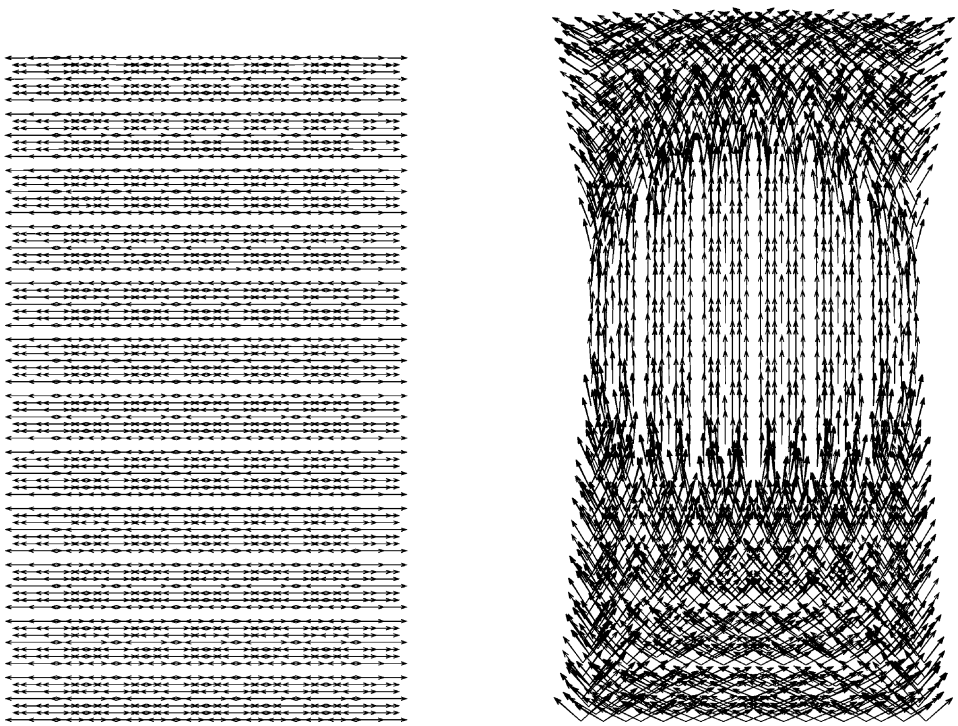

Fig. 8. The polarization of the individual finite elements projected onto the *xz* plane (a) in the absence of an electric field, and (b) with an electric field of 120 MV/m along the *z*-axis. The regular spacing in the *z* direction is related to the tetragonal element shape in the 3D meshing and not to a physical property.

getics. The central switched region aligned with the electric field lowers the energy of the system. If the sample has total height h and a square base of area b^2, then the energy due to the dipole moments of the piezoelectric interacting with the external electric field is approximately $-p_0Eb^2(h-2\Delta h)$, where p_0 is the dipole moment per unit volume in the tetragonal phase, and E is the external electric field. In the region that has switched, we neglect elastic energy since it will be close to the tetragonal phase. Over the distance Δh the horizontal cross section of the piezoelectric narrows from its value at the plates to that of the central (switched) region. This creates competition between two kinds of elastic deformation. Here we treat the sample as a homogeneous elastic body. The elastic energy due to stretch in the region, U_ε, favors small Δh, whereas the elastic energy due to shearing, U_γ favors large Δh. We estimate $U_\varepsilon \approx C\varepsilon^2 b^2 \Delta h$ and $U_\gamma \approx C\gamma^2 b^2 \Delta h$, where ε and γ are the normal and shear strains, respectively, and C is the elastic constant[3]. We can estimate $\varepsilon \approx \Delta b/b$ and $\gamma \approx \Delta b/\Delta h$, where Δb is half the difference between the length of the surface which is in contact with the plates and the narrower (switched) bulk region (see Fig.

[3] This approximation neglects the multiple-well energy surface of a piezoelectric. A multiple well energy surface can be approximated by using the elastic constants, the distance in strain space between the tetragonal wells, and the order of magnitude of the barrier between the tetragonal wells obtained from elastic band calculations. Even if the range of strains is large enough to sample two tetragonal wells (one at the plates and another at a distance Δh from the plates), when integrated over the entire sample our simple elastic approximation and the multiple well model are different at most by an order of magnitude, an error acceptable given the qualitative nature of our model. For the same reason we also neglect the difference between the shear and normal elastic moduli.

5). Considering the sample as a whole, the total potential energy is

$$U_{\text{tot}} \approx C\varepsilon^2 b^2 \Delta h + C\gamma^2 b^2 \Delta h - p_0 E b^2 (h - 2\Delta h) - \Delta W, \quad (6)$$

where ΔW is the work done by the system. We estimate that the work for the sample to expand against the plates (actuate) as $2b^2\sigma_0(\Delta b_0/b)(h-2\Delta h)$, where σ_0 is the external normal stress and Δb_0 is the value of Δb when the surfaces are pinned. The sample also does work if it slides against the plates, which we label ΔW_s. The work of sliding depends explicitly on Δb but not on Δh. Using the reduced variables $\beta \equiv \Delta b/b$, $\zeta \equiv \Delta h/b$, and $\eta \equiv h/b$, we can write the total energy,

$$\frac{1}{b^3}U_{\text{tot}}(\beta,\zeta) \approx C\beta^2\zeta + C\frac{\beta^2}{\zeta} - p_0 E(\eta - 2\zeta) + \sigma_0\beta_0(\eta - 2\zeta) - W_s(\beta). \quad (7)$$

Eq. (7) can be considered an approximation of the energy functional used in the simulation. Minimizing Eq. (7) with respect to ζ gives,

$$\zeta = \left[\frac{C}{C + (2p_0E - 2\beta_0\sigma_0)/\beta^2}\right]^{\frac{1}{2}}. \quad (8)$$

We compare the relative orders of magnitude of the quantities in Eq. (8) to determine the important terms. For $PbTiO_3$ the elastic constants are on the order of 10^2 GPa and the polarization density in the tetragonal phase is on the order of 1 C/m^2 (see Fig. 2 and Ref. [16]). For the simulations described above, $\beta = \beta_0 \approx 10^{-1}$, $E \approx 10^8$ V/m, and $\sigma_0 \approx 10^8$ Pa. Taking all these together, we find $p_0E/\beta^2 \approx 10$ GPa, while the work term proportional to σ_0 is an order of magnitude smaller. The denominator in Eq. (8) is thus dominated by the elastic constant and we expect $\zeta \approx 1$, which is what is observed in the simulations. Note that the elastic constants, polarization density, and β_0 are the only material properties that enter into this simple model; details about the complicated energy landscape of $PbTiO_3$ are not important.

We can also apply this model to the experimental system, where the sample is not pinned to the plates. In the experiments the sample is a thin single-crystal plate, with h=0.2b. Actuation strains of 70% of the theoretical limit are achieved [4], which suggests that $\Delta h < 0.2\,h$, so the experimental system is in the regime $\zeta \ll 1$. According to Eq. (8) this requires $\beta^2 \ll (p_0E - \beta_0\sigma_0)/C$. In the experiments $E \approx 10^6$ V/m and $\sigma_0 \approx 10^6$ Pa. For $BaTiO_3$, $p_0 \approx 10^{-1}$ C/m^2, $\beta_0 \approx 10^{-2}$, and $C \approx 10^{11}$ N/m^2 [28]. These values imply that $\beta \ll 10^{-3}$, indicating that $\beta \ll \beta_0$ which means that the entire sample is completely switched to align with the z-axis. Thus as the electric field cycles, the sample as a whole contracts and expands and its surfaces slide back and forth against the plates.

The complete switching predicted by the model is curious since in the experiments, the actuation strain is 30% less than the theoretical maximum. The qualitative treatment of the energy in Eq. (6) leaves out important aspects of the experimental system such as cracking and the dynamics of switching as the electric field changes; however, the analysis suggests that friction alone cannot explain the 30% deficit in the actuation of the experimental system. This conclusion is supported by the experimental curve presented in Ref. [4]. If friction were an important limiting factor in the strain, after the polarization aligns with the electric field, one might expect the strain to increase as the electric field does. This does not appear to be happening in any substantial way over the first cycle in the experiment.

6. Conclusions

We implemented the ab initio model of $PbTiO_3$ of Ref. [16] within a finite element formulation to simulate macroscopic switching response. We presented a variational principle with appropriate electric boundary conditions for closed-circuit conditions.

First, the model was used to simulate polarization switching under uniform mechanical and electrical loading. The switching mechanism was studied using the elastic band method to estimate transition paths and barriers. The results suggest that 180° switching may be effected through two consecutive 90° switches. The reason for this is that the energy barrier for the 90° switch is more than an order of magnitude smaller than the barrier for a direct 180° switch. This result quantitatively validates the assumption made in the phenomeno-

logical models used in earlier FEM work on piezoelectrics [5].

Values were obtained for the critical switching fields for 90° and 180° switching and the critical stress for stress-induced 90° switching. The switching fields and stresses predicted by our model are much larger than experimental values for related materials. The fact that, unlike the materials used in experiments, $PbTiO_3$ is far from its phase transition can partly explain the discrepancy. It is also well-known from experiments that inhomogeneities in the sample, due to domain walls and grain boundaries, can play an important role in the piezoelectric response of a material. The analysis in the present work does not include any sample inhomogeneities which is a simplification of the problem and indicates the need for more accurate treatment in the future.

Finally, we applied our method to investigate the high-strain actuator proposed by Shu and Bhattacharya [27]. We qualitatively reproduced the experimental strain vs. electric field curve for this actuator [4], and explored how changes in applied stress affect the behavior of the system. We also explored, via simulation and a simple model, how friction between the plates and the sample affects the polarization field and switching behavior of the actuator. From our theoretical analysis we suggested that in the experimental system the ferroelectric crystal slides back and forth against the plates during cycling of the electric field, despite the friction between the plates and crystal. However, we noted aspects of our theoretical model that require further work.

Future work will focus on extending our model. The main advantage of our simulation method is that it is based on first-principles calculations with no adjustable parameters. In that sense the simulations are predictive and any shortcomings are a result of physical aspects of the problem that have been left out. The main effects left out are sample inhomogeneities and the kinetics of switching. Inhomogeneities may be accounted for by application of the full nonlocal formalism of the quasicontinuum method [29]. Kinetics can only be treated in a phenomenological manner at this stage, perhaps by using an approach similar to the domain evolution method of Loge and Suo [30].

Acknowledgements

This work was supported by Harvard University's Materials Science and Engineering Center, which is funded by the NSF. It is a pleasure to acknowledge helpful discussions with K. Bhattacharya and J. R. Rice.

References

[1] Devonshire AF. Phil Mag Suppl 1954;3:85.
[2] Auciello O, Scott JF, Ramesh R. Physics Today 1998;51(7):22.
[3] Busch-Vishniac IJ. Physics Today 1998;51(7):28.
[4] Burcsu E, Ravichandran G, Bhattacharya K. Appl Phys Lett 1698;2000:77.
[5] Hwang SC, McMeeking RM. Ferroelectrics 1998;207:465.
[6] Cao H, Evans AG. J Am Ceram Soc 1993;76:890.
[7] Allik H, Hughes TJR. Int J Numer Meth Eng 1970;2:151.
[8] Lerch R. IEEE Trans. on Ultrasonics, Ferroelectrics and Frequency Control 1990;37(May):233.
[9] Hom CL, Shankar N. J Intell Mater Syst and Struct 1994;5:795.
[10] Gong X, Suo Z. J Mech Phys Solids 1996;44:751.
[11] Piquette JC, Forsythe SE. J Acoust Soc Am 1997;101:289.
[12] Debus J-C, Dubus B, Coutte J. J Acoust Soc Am 1998;103:3336.
[13] Chen W, Lynch CS. Acta Mater 1998;46:5303.
[14] Chen X, Fang DN, Hwang KC. Acta Mater 1997;45:3181.
[15] Vanderbilt D. Current Opinions in Solid State and Materials Science 1997;2:701.
[16] Waghmare UV, Rabe KM. Phys Rev B 1997;55:6161.
[17] Tadmor EB, Smith GS, Bernstein N, Kaxiras E. Phys Rev B 1999;59:235.
[18] King-Smith RD, Vanderbilt D. Phys Rev B 1994;49:5828.
[19] Resta R. Rev Mod Phys 1994;66:899.
[20] Malvern LE. Introduction to the mechanics of a continuous medium. Englewood Cliffs: Prentice-Hall, 1969.
[21] Landau LD, Lifshitz EM. Statistical physics. Oxford: Pergamon Press, 1963.
[22] Papadrakakis M, Gantes CJ. Int J Numer Meth Eng 1989;28:1299.
[23] Lines ME, Glass AM. Principles and applications of ferroelectrics and related materials. Oxford: Oxford University Press, 1977 Chapter 8.
[24] Foster CM, Bai G-R, Csencsits R, Vetrone J, Jammy R, Willis LA et al. J Appl Phys 1997;81:2349.
[25] Landauer R, Young DR, Drougard ME. J Appl Phys 1956;27:752.
[26] Elber R, Karplus M. Chem Phys Lett 1987;139:375.
[27] Shu, Y.C., Bhattacharya, K., submitted to Phil. Mag. A.
[28] Li Z, Foster CM, Dai X-H, Xu X-Z, Chan S-K, Lam DJ. J Appl Phys 1992;71:4481.
[29] Shenoy VB, Miller R, Tadmor EB, Rodney D, Phillips R, Ortiz M. J Mech Phys Solids 1999;47:611.
[30] Loge RE, Suo Z. Acta Mater 1996;44:3429.